Facile electrodeposition of high-density $CuCo_2O_4$ nanosheets as a high-performance Li-ion battery anode material

S. M. Pawar,[a] B. S. Pawar,[a] Bo Hou,[b] ATA Ahmed,[a] H. S. Chavan,[a] Yongcheol Jo,[a] Sangeun Cho,[a] Jongmin Kim,[a] Jiwoo Seo,[a] SeungNam Cha,[b] A. I. Inamdar,[a] Hyungsang Kim,[a] and Hyunsik Im[a]

[a] Division of Physics and Semiconductor Science, Dongguk University, Seoul 04620, South Korea

[b] Department of Engineering Science, University of Oxford, Parks Road, OX1 3PJ, UK

Abstract

High-density $CuCo_2O_4$ nanosheets are grown on a nickel foam (NF) substrate using an electrodeposition method followed by air annealing for use as a lithium-ion (Li-ion) battery anode material. It exhibits a high discharge capacity of 1244 mA/g at 0.1 A/g with a coulombic efficiency of 82 %. The $CuCo_2O_4$ nanosheet anode shows excellent high-rate performance and stability with 95% capacity retention (1100 mAh/g) at 1 A/g after 200 cycles. The superior electrochemical performance of the $CuCo_2O_4$ nanosheet electrode is attributed to the binder-free direct contact of the electrode active material to the current collector and unique high-density nanosheet morphology.

Keywords: $CuCo_2O_4$ nanosheets, electrodeposition, Li-ion battery, cyclic voltammetry, anode material

E-mail: spawar81@gmail.com (S.M. Pawar), hskim@dongguk.edu (H. Kim), hyunsik7@dongguk.edu (H. Im)

Introduction

The increasing concern over energy crisis and environmental pollution from burning fossil fuels has significantly driven the development of clean and renewable energy sources [1]. Among the various energy storage devices, regardless of lithium (Li) scarcity, rechargeable Li-ion batteries (LIBs) are still considered as the most efficient energy storage device at the present time, due to their high energy density, long-term stability, and environmental friendliness [1-2]. For commercially available LIBs, graphite is commonly used as an anode material due to its low price, high conductivity, and high reversibility [3]. However, it has a low theoretical capacity (372 mAh/g) and serious safety issues have arisen from Li dendrite formation, which limits the large-scale application [4]. Therefore, considerable attention is being paid to explore alternative anode materials with high capacity along with excellent cycling stability and rate capability.

Recently, many ternary transition metal oxides including $NiCo_2O_4$, $CuCo_2O_4$, and $ZnCo_2O_4$ have been extensively studied for use as LIB anode materials due to their low cost, high specific capacity and good stability. The observed high performance of the materials is understood in terms of the synergetic effects between the two constituting transition metal elements during the Li+ discharge/charge process [2,3]. Among these, more attention has been paid to spinel copper cobaltite ($CuCo_2O_4$) because of its abundance and environmental friendliness. Various nanostructured $CuCo_2O_4$ anode materials ranging from nanoparticles, hollow spheres, nanorods, and nanocubes have been reported [5-12]. Table 1 reports the LIB performance of various nanostructured $CuCo_2O_4$. Two-dimensional (2-D) nanostructures exhibit a better electrochemical performance than other nanostructures due to short Li+ diffusion pathways, large electrochemically active sites and low diffusive resistance at the

electrode/electrolyte interface [13,14]. In order to enhance the anode performance of $CuCo_2O_4$, it is desirable to fabricate nanostructured 2-D $CuCo_2O_4$ directly deposited on the current collector.

In this work, we report the facile electrodeposition of $CuCo_2O_4$ nanosheets on a nickel foam (NF) substrate for use as a binder-free anode for LIB. The $CuCo_2O_4$ nanosheet anode exhibits a high specific capacity of ~1244 mAh/g at 0.1 A/g along with excellent cycling stability and high rate capability.

Experimental

Fabrication of $CuCo_2O_4$ nanosheet film

A copper-cobalt hydroxide (Cu-$Co(OH)_2$) precursor film was prepared on NF substrate using an electrodeposition method at room temperature. The precursor solution was prepared using 2.5 mM copper nitrate ($(Cu(NO)_3)_2.3H_2O$) and 10 mM cobalt nitrate ($(Co(NO_3)_2).6H_2O$) solutions. Analytical reagent grade chemicals were used for the precursor solution preparation (supplied by Sigma-Aldrich). Prior to the electrodeposition, the NF substrate was cleaned with a 3 M HCl solution using ultra-sonication for 10 min to remove the nickel oxide layer. The NF substrate was washed with acetone, ethanol and distilled water for 10 min and then it was dried at 60 °C for 24 h in the air environment. The electrodeposition was carried out using a conventional three-electrode cell where a Pt wire was used as the counter electrode, while the saturated calomel electrode (SCE) and an NF substrate with an area of 2×4 cm^2 served as the reference electrode and the working electrode, respectively.

A $CuCo(OH)_2$ precursor film was deposited at -1.0 V (vs. SCE) in potentiostatic mode (VERSA-STAT3, Princeton Applied Research) for 300 s. Afterward, the deposited film was

rinsed with deionized water and then dried at room temperature. The deposited film was annealed in an air atmosphere at 300 ^{0}C with a ramping rate of 2 °C/min for 2 h.

Materials characterization

The structural and chemical properties of the annealed film were studied using high resolution X-ray diffraction (XRD) with Ni-filtered CuKα radiation [kα = 1.54056 Å] (X_pert PRO, Philips, Eindhoven, Netherlands) and X-ray photoelectron spectroscopy (XPS, VG Multilab 2000, Thermo VG Scientific, UK) with a monochromatic Mg-Kα (1253.6 eV) radiation source, respectively. The surface morphology, chemical composition, and crystallinity of the sample were examined using field emission scanning electron microscope (FE-SEM, Model: JSM-6701F, JEOL, Japan), energy-dispersive X-ray spectroscopy (EDS), transmission electron microscopy (TEM, JEOL 2010), and selected area electron diffraction (SAED), respectively.

Electrochemical Measurements

The $CuCo_2O_4$ film on NF was punched into circular plates with a diameter of 12 mm, and served directly as the working electrode. For the evaluation of the electrochemical properties of the $CuCo_2O_4$ nanosheet anode, a CR2032-type coin cell was assembled in an argon gas glove box (KOREA KIYON), in which, both H_2O and O_2 levels were kept below 0.1 ppm. Lithium metal foil was used as the counter electrode (cathode), a Celgard 2300 microporous membrane was used as the separator and 1M $LiPF_6$ dissolved in a mixture of ethylene carbonate and dimethyl carbonate (1:1 vol %) was used as the electrolyte solution. The electrochemical properties of the $CuCo_2O_4$ anode were studied using cyclic voltammetry (CV), galvanostatic

charge-discharge, and electrochemical impedance spectroscopy (EIS) using a Bio-Logic (MPG-2) battery cycler.

Results and discussion

A brownish bimetallic (Cu,Co) hydroxide precursor film was co-electrodeposited on the NF surface through the reactions of (Cu^{2+}, Co^{2+}) ions with OH^-, originated from the reduction of NO_3^- at the positive electrode. The generation of OH^- ions during the electrodeposition process were raised the local pH value, resulting in the uniform precipitation of mixed (Cu, Co) hydroxide on the NF surface. After this, (CuCo) hydroxide was thermally transformed into $CuCo_2O_4$ on the NF substrate. The corresponding electrochemical reactions are described as follows [15,16]:

$$NO_3^- + 7H_2O + 8e^- \rightarrow NH_4^+ + 10\ OH^- \quad (1)$$

$$xCu^{2+} + 2xCo^{2+} + 6xOH^- \rightarrow Cu_xCo_{2x}(OH)_{6x} \quad (2)$$

$$Cu_xCo_{2x}(OH)_{6x} + ½\ xO_2 \rightarrow xCuCo_2O_4 + 3x6H_2O \quad (3)$$

Fig. 1(a) shows the XRD pattern of the $CuCo_2O_4$ nanosheets on the NF substrate. It contains three strong peaks indicated by "#", corresponds to the NF substrate. The as-deposited $CuCo(OH)_2$ precursor film does not show any diffraction peaks, revealing its amorphous nature (Fig. S1). The clear diffraction peaks at 31.40º, 37.0º, 39.0º, 59.48º and 65.54º are observed and indexed to the (220), (311), (222), (511) and (440) planes of the spinel cubic $CuCo_2O_4$ phase, respectively (JCPDS card no. 01-1155). No other impurity peaks are observed.

The composition and oxidation states of the $CuCo_2O_4$ nanosheets were characterized using EDS and XPS measurements. The atomic ratio of Cu to Co in the annealed sample is ~ 1:2

(Table S1). The survey XPS spectrum (Fig. S2) shows the presence of Cu, Co, and O with the carbon (for calibration). Fig. 1 (b-d) depicts the deconvoluted core-level spectra of Cu 2p, Co 2p, and O 1s, respectively. The core-level Cu 2p spectrum consists of two main peaks at binding energies of 933.5 and 953.4 eV. In addition, two shake-up satellite peaks (indicated by "Sat.") are also observed at 942.1 and 962.1 eV (Fig. 1b), confirming the characteristic Cu^{2+} [17]. The Co 2p peak is deconvoluted into Co $2p_{3/2}$ and Co $2p_{1/2}$ spin-orbit doublets at 779.8 and 794.8 eV, respectively (Fig. 1c), together with a spin-energy separation of 15 eV, indicating the presence of mixed Co^{2+} and Co^{3+}. The presence of the two shake-up satellite peaks reveal that cobalt has a spinel structure [18]. The deconvoluted spectrum of O 1s in Fig 1d consists of three components. The O1 component at 529.4 eV corresponds to metal-oxygen bonds. The well-resolved O2 component at 531.2 eV is associated with a larger number of defect sites with low oxygen coordination. The O3 component at 532.6 eV is assigned to the multiplicity of physi-sorbed and chemi-sorbed water at or near the surface [19].

Fig. 2 (a) shows the FE-SEM image of the $CuCo_2O_4$ nanosheets. The uniform nanosheets are vertically formed on the NF substrate and interconnected to each other. The thickness of the nanosheets is about 10 -15 nm. This unique morphology is beneficial for ionic transport as well as electron transfer. The morphology of the as-deposited $CuCo(OH)_2$ nanosheets does not change after annealing (Fig. S3). It is seen that the nanosheets are porous in nature (Fig. 2 (b)). From the HR-TEM analysis shown in Fig. 2(c), the spacing between adjacent planes is found to be ~ 0.14 nm which corresponds to the (440) plane of $CuCo_2O_4$ and is in agreement with the XRD data. The corresponding selected-area electron diffraction (SAED) pattern (Fig. 2d) exhibit well-defined diffraction rings with (111), (311) and (222) planes, revealing that the prepared material

is spinel $CuCo_2O_4$ with a polycrystalline nature. Moreover, uniform distribution of the Cu and Co elements in the desired composition are observed in the film (Fig. 2 (e) and Table S1)

Fig. 3a shows the cyclic voltammetry curves (CVs) for the $CuCo_2O_4$ nanosheet electrode for the 1st, 2nd, 3rd, and 4th cycles at a scan rate of 0.1 mV/s. In the cathodic scan of 1st cycle, two well-defined strong reduction peaks are observed at 1.0 and 0.7 V, which correspond to the reduction of Co^{3+} to Co^{2+} to metallic Co or Cu nanoparticles, respectively and formation of a solid electrolyte interface (SEI) layer[8,12]. In the anodic scan, two broad oxidation peaks are found at ~1.55 and ~2.10 V, which can be attributed to the oxidation of metallic Co and Cu into Co_3O_4 and CuO, respectively [5]. Similarly, the 2nd, 3rd and 4th CV curves indicate a good reversibility of the redox reaction. Because of the irreversible electrochemical reaction and the SEI layer formation after the 1st discharge cycle, the reduction peaks shift towards a higher potential side. On the contrary, the oxidation peaks are observed at similar potential values. The electrochemical reactions involved in this processes are as follows [8, 12]:

$$CuCo_2O_4 + 8\,Li^+ + 8\,e^- \rightarrow Cu + 2Co + 4\,Li_2O \quad (4)$$

$$Cu + Li_2O \rightarrow CuO + 2Li^+ + 2e^- \quad (5)$$

$$2Co + 2Li_2O \rightarrow 2CoO + 4Li^+ + 4e^- \quad (6)$$

$$6CoO + 2Li_2O \rightarrow 2Co_3O_4 + 4Li^+ + 4e^- \quad (7)$$

Fig. 3 (b) shows the galvanostatic charge-discharge curves up to the 4th cycle at a constant current density of 0.1A/g. There are two discharge voltage plateaus at 1 and 0.7 V in the first curve whereas the charge voltage plateaus feature is observed at 1.55 and 2.10 V. These results are in good agreement with the potentials for the oxidation and reduction peaks in the 1st CV curve. The initial discharge and charge capacities are about 1244 and 1020 mAh/g, with a coulombic efficiency of 82 %. In the 2nd, 3rd and 4th cycles, the discharge potential plateaus shift

towards a higher potential and the long discharge potential plateau changes to a sloping discharge curve, indicating that a stable SEI is formed during the 1st cycle [20].

The rate capability of the electrode was measured with different current densities for each of five cycles and the results are shown in Fig. 3(c). As the current density increases up to 10 A/g, the discharge capacity decreases gently, thus showing an excellent high rate performance. As the current density recover to 1A/g, the discharge capacity (~1150 mAh/g) increases by ~ 12 % compared with the initial value (988 mAh/g) at the same current density. The increased capacity might have been associated with the phenomenon that the electrode material either partially loses its crystallinity or transforms to an amorphous-like structure during the cycling [21]. Fig. 3 (d) shows the cycling performance of the $CuCo_2O_4$ nanosheet electrode at a constant current density of 1 A/g for 200 cycles. The capacity of the electrode gradually decreases up to 90 cycles. After words, the capacity almost recovers to its initial value, presumably due to the activation of the electrode, the electrolyte decomposition or the formation of the SEI [22]. The $CuCo_2O_4$ nanosheet electrode exhibits a capacity retention of 95% (1100 mAh/g) after 200 cycles.

The EIS spectra were measured to understand the performance of the $CuCo_2O_4$ nanosheet electrode for before and after stability test. Fig. 4 shows the Nyquist plots obtained from the $CuCo_2O_4$ nanosheet electrode for fresh cell and after the stability test. Both the Nyquist plots exhibit a semicircles in the high-frequency region and a straight line in the low-frequency region. The straight line in the low-frequency region corresponds to the Warburg impedance (Z_W) and the semicircle are associated with the diffusion of Li+ ions into the electrode and the charge transfer resistance(Rct), respectively[22]. Moreover, the solution resistance (Rs) as well as Rct after the stability test is increased. Which can be attributed to the formation of a passivation layer due to the decomposition of the electrolyte [23].

Conclusions

A binder-free $CuCo_2O_4$ nanosheet anode for LIB has been successfully synthesized on NF substrate using an electrodeposition method followed by air annealing at 300 °C. The initial discharge specific capacity of the $CuCo_2O_4$ anode is 1244 mAh/g at 0.1 mA/g with a good coulombic efficiency of 82%. Also, it shows excellent high rate performance and stability with a capacity retention of 95% (1100 mAh/g) at a constant current density of 1 A/g after 200 cycles. Considering the facile synthesis as well as the excellent battery anode performance, the $CuCo_2O_4$ nanosheet film in the present study has the potential to be an alternative to the current anode electrodes in LIB applications.

Acknowledgments

The authors would like to thank the financial support from the National Research Foundation (NRF) of Korea (Grant nos. 2015M2A2A6A02045251, 2018R1A2B6007436, 2016R1A6A1A03012877, and 2015R1D1A1A01060743).

References:

[1] V. Etacheri , R. Marom , R. Elazari , G. Salitra, D. Aurbach, Energy Environ. Sci. 4 (2011) 3243-3262.

[2] F. Zhang, L. Qi, Adv. Sci. 3 (2016) 1600049.

[3] K. Cao, T. Jin, L. Yang, L. Jiao, Mater. Chem. Front. 1 (2017) 2213-2242.

[4] D. P. Dubal, D.R. Patil, S.S. Patil, N. R. Munirathnam, P. Gomez-Romero , ChemSusChem 10 (2017) 4163-4169.

[5] Y. Sharma, N. Sharma, G.V. Subba Rao, B.V.R. Chowdari, Journal of Power Sources 173 (2007) 495-501.

[6] F. Jiang, Q. Su, H. Li, L. Yao, H. Deng, G. Du ,Chemical Engineering Journal 314 (2017) 301-310.

[7] S. Cai, G. Wang, M. Jiang, H. Wang, Solid State Electrochem 21 (2017) 1129-1136.

[8] H.S. Jadhav, S. M. Pawar, A. H. Jadhav, G. M. Thorat,J. G. Seo, Scientific Reports 6 (2016) 31120.

[9] J. Ma, H. Wang, X.Yang, Y. Chai,R. Yuan, J. Mater. Chem. A 3 (2015) 12038–12043.

[10] H. Zhang, Z. Tang, K. Zhang, L. Wang, H. Shi, G. Zhang, H. Duan, Electrochim. Acta 247 (2017) 692-700.

[11] W. Kang, Y. Tang, W. Li, Z. Li, X.Yang, J. Xu, C.-S.Lee, Nanoscale 6 (2014) 6551-6556

[12] M. Bhardwaj, A. Suryawanshi, R. Fernandes, S. Tonda, Abhik Banerje, D. Kothari, S. Ogale, Materials Research Bulletin 90 (2017) 303-310.

[13] F.Zheng, D. Zhu, Q.Chen, ACS Appl. Mater. Interfaces 6 (2014) 9256-9264.

[14] L. Zhao, L. Wang,P. Yu, C. Tian, H. Feng, Z. Diao,H. Fu, Dalton Trans.46 (2017) 4717-4723

[15] C. Yuan, L. Yang, L. Hou, L. Shen, X. Zhang, X. W. Lou, Energy Environ. Sci.5 (2012) 7883-7887.

[16] L. Abbasi, M. Arvand, Applied Surface Sci. 445 (2018) 272-280.

[17] S. Liu, K. S. Hui, K. N. Hui, ACS Appl. Mater. Interfaces 8 (2016) 3258-3267.

[18] Q. Liao,N. Li, S.Jin, G. Yang,C. Wang, ACS Nano 9 (2015) 5310-5317.

[19] Y. Lei, J. Li, Y. Wang, L. Gu, Y. Chang, H. Yuan and D. Xiao, ACS Appl. Mater. Interfaces 6 (2014) 1773-1780.

[20] D. Deng, J.Y. Lee, Nanotechnology 22 (2011) 355401-355409.

[21] S.Sun, Z.Wen, J.Jin, Y.Cui, Y.Lu, Microporous and Mesoporous Materials 169 (2013) 242- 247.

[22] A. I. Inamdar, R. S. Kalubarme, J. Kim, Y. Jo, H. Woo, S. Cho, S. M. Pawar, C.-J. Park, Y.-W. Lee, J. I. Sohn, S. Cha, J. Kwak, H. Kim, H. Im, J. Mater. Chem. A 4 (2016) 4691-4699.

[23] Y. Wang, J. Roller, R. Maric, Journal of Power Sources 378 (2018) 511-515.

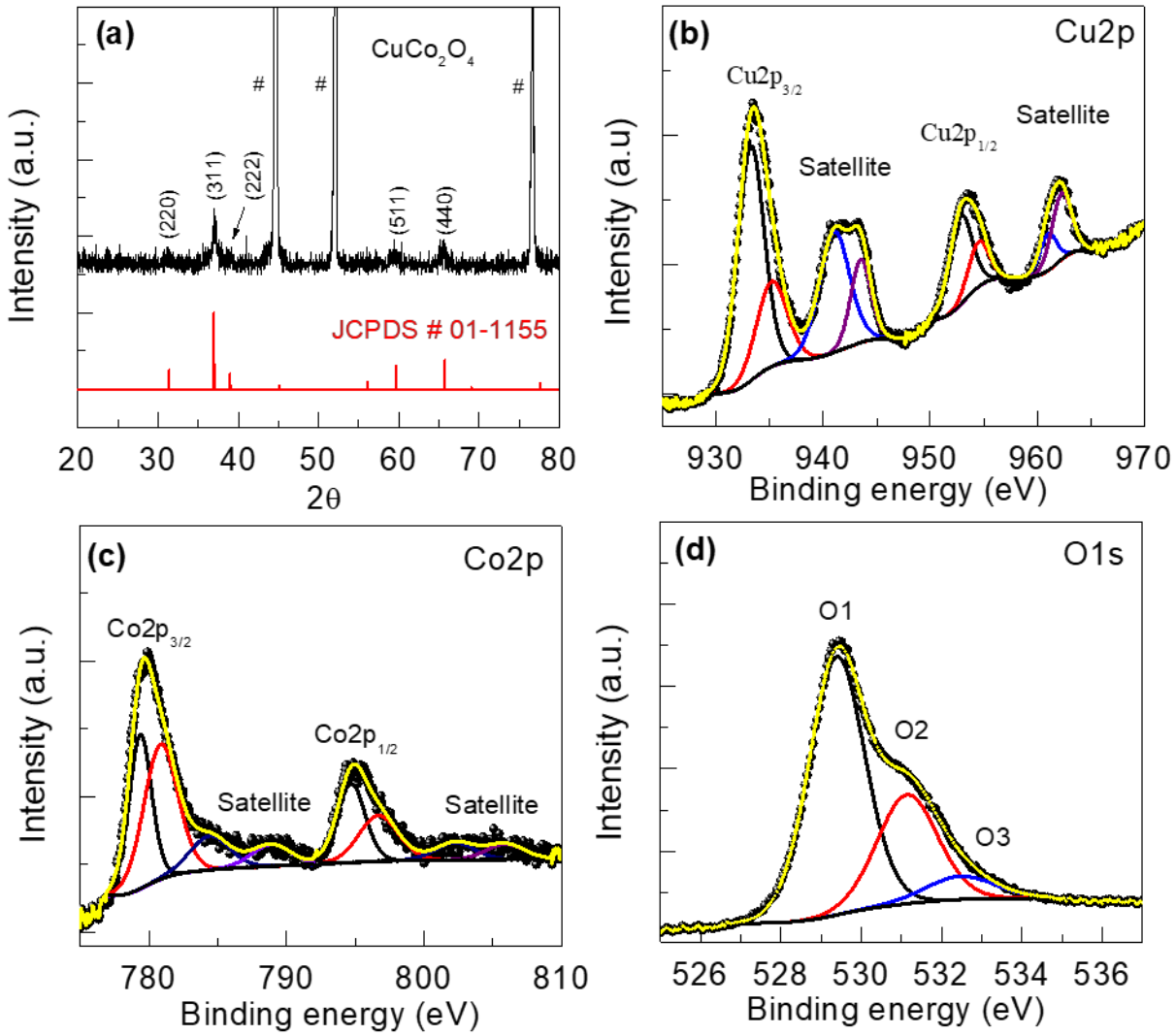

Fig. 1. (a) X-ray diffraction pattern, (b) Cu2p (c) Co2p and (d) O1s spectra of the $CuCo_2O_4$ nanosheet film.

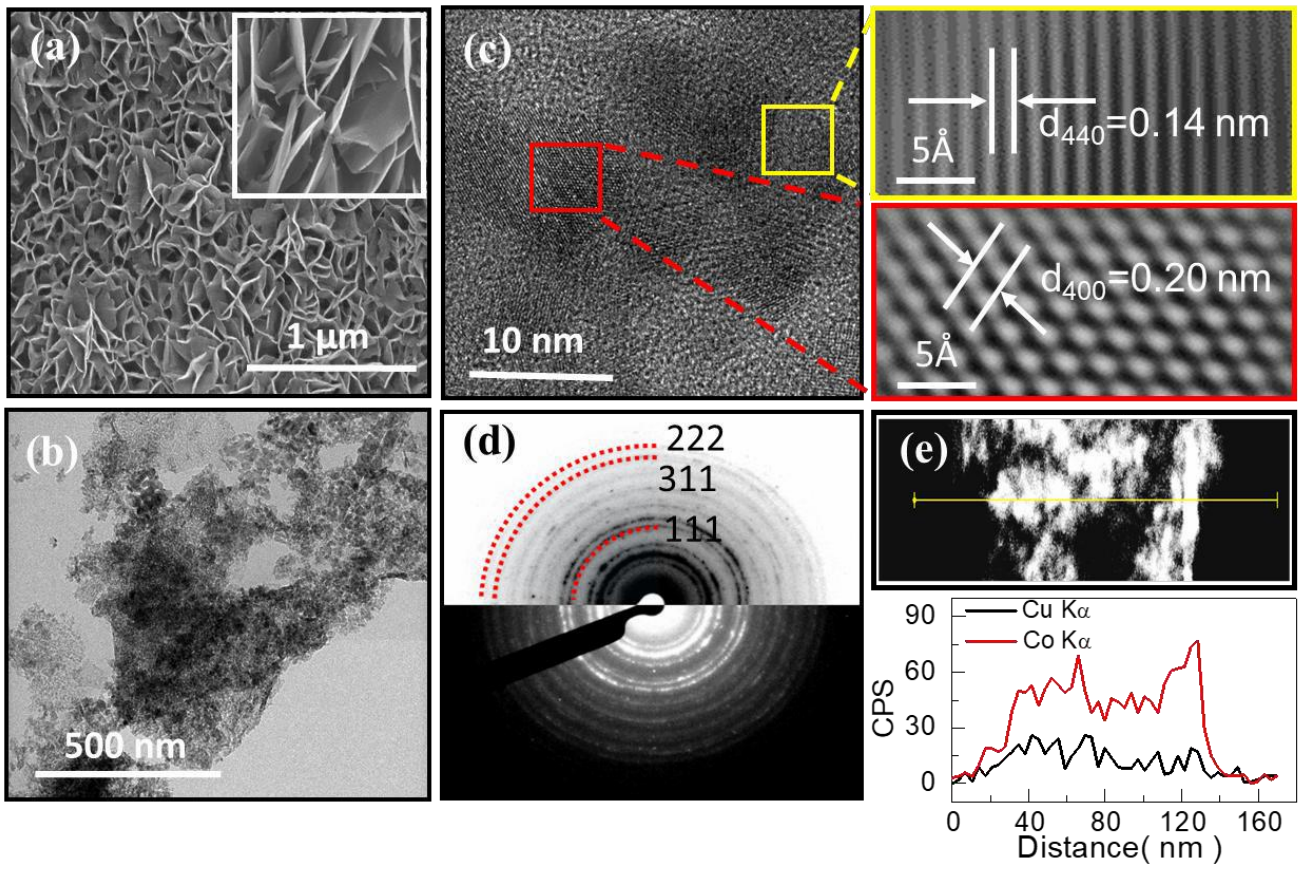

Fig. 2. (a) FE-SEM image (inset is high magnification), (b)TEM image, (c)HR-TEM image (inset is high magnification), (d) SAED pattern and (e) EDS elemental mapping with line scanning of the $CuCo_2O_4$ nanosheet film.

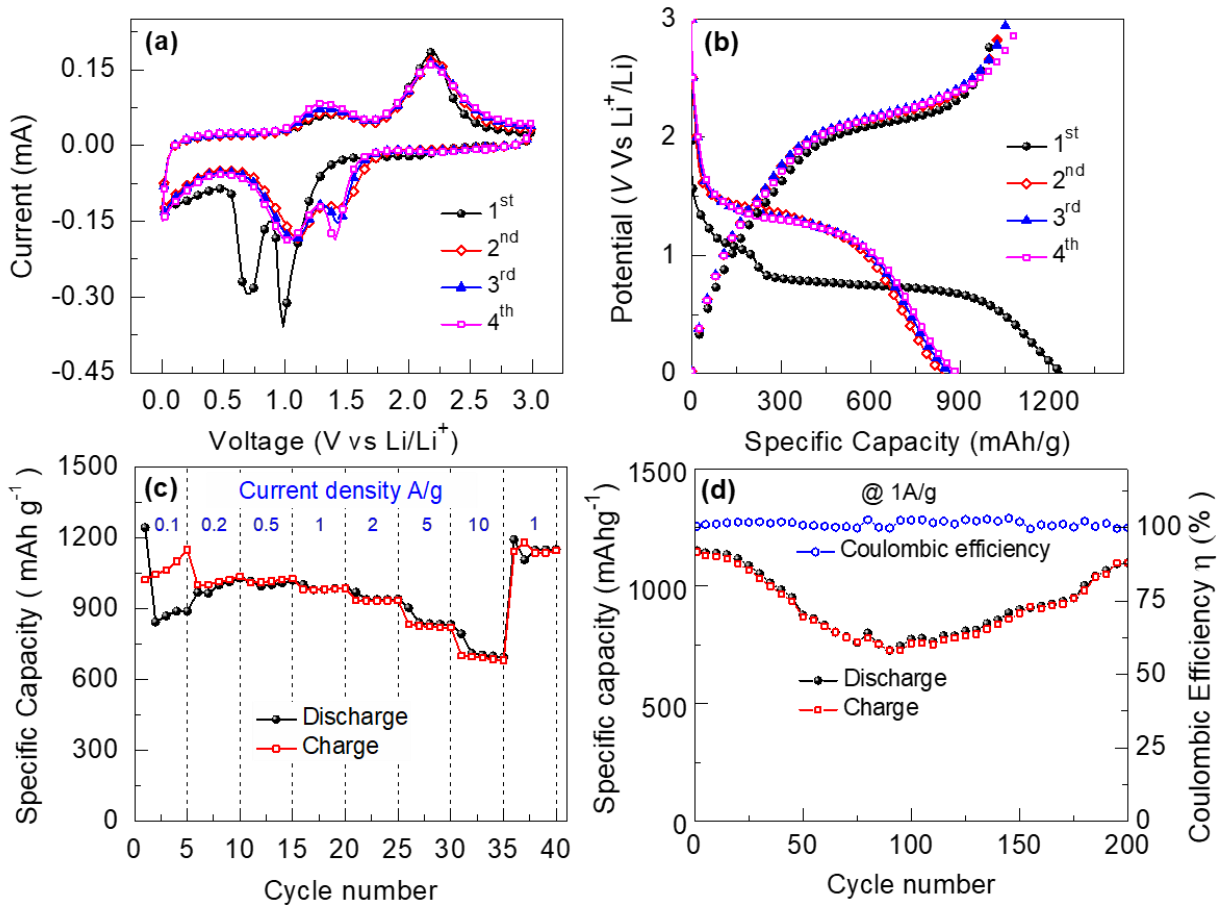

Fig. 3. (a) Cyclic voltammograms (CV) at a scan rate of 0.1 mV/s, (b) Galvanostatic charge /discharge curves at 0.1 A/g for fist 4 cycles, (c) Rate capability measured at various current densities, and (d) cycling performance of the $CuCo_2O_4$ nanosheet electrode.

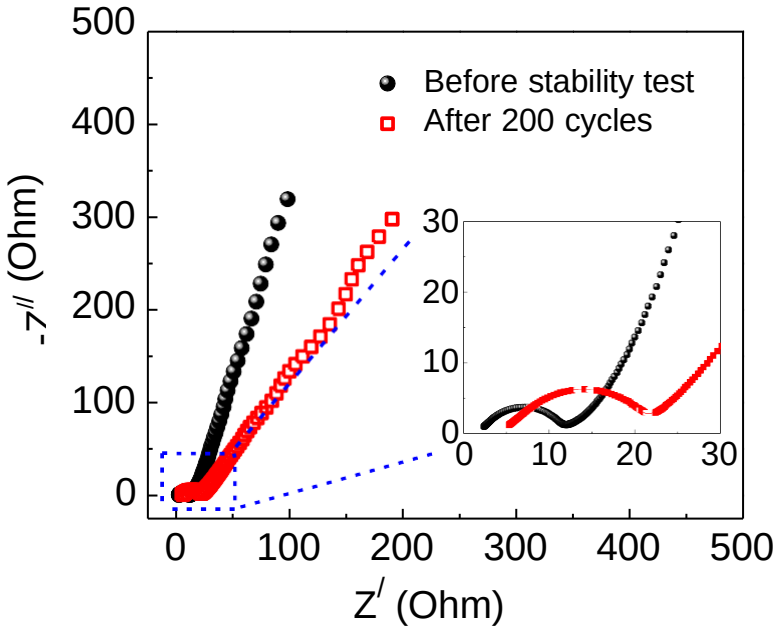

Fig. 4. Nyquist plots of the $CuCo_2O_4$ nanosheet electrode before and after 200 galvanostatic charge /discharge cycles.

Table 1: A LIB performance comparison between the various nanostructured $CuCo_2O_4$ - based anode materials

Morphology	Method	Specific capacity ($mAhg^{-1}$)	Current density ($A\ g^{-1}$)	Cycle number	Ref.
$CuCo_2O_4$ nanoparticle	combustion	755	0.06	20	[5]
$CuCo_2O_4$ nanoparticle/Graphene nanosheet	Solvothermal	1040	@0.1C	80	[6]
$CuCo_2O_4$ hallow sphere	hydrothermal	930	0.1	150	[7]
3D $CuCo_2O_4$ flower	Hydrothermal	1160	1	200	[8]
Carbon coated $CuCo_2O_4$ concave polyhedron	Water bath	740	@0.1C	50	[9]
$CuCo_2O_4$/C nanofiber	electrospinning	865	0.2	400	[10]
$CuCo_2O_4$ nanocubes /rGO	Microwave assisted solvothermal	570	1	350	[11]
$CuCo_2O_4$ nanowall	hydrothermal	550	@0.375C	120	[12]
$CuCo_2O_4$ nanosheet	electrodeposition	1100	1	200	This work

Supporting Information

Facile electrodeposition of high-density $CuCo_2O_4$ nanosheets as a high-performance Li-ion battery anode material

S. M. Pawar,[a] B. S. Pawar,[a] Bo Hou,[b] ATA Ahmed,[a] H. S. Chavan,[a] Yongcheol Jo,[a] Sangeun Cho,[a] Jongmin Kim,[a] Jiwoo Seo,[a] SeungNam Cha,[b] A. I. Inamdar,[a] Hyungsang Kim,[a] and Hyunsik Im[a]

[a] Division of Physics and Semiconductor Science, Dongguk University, Seoul 04620, South Korea

[b] Department of Engineering Science, University of Oxford, Parks Road, OX1 3PJ, UK

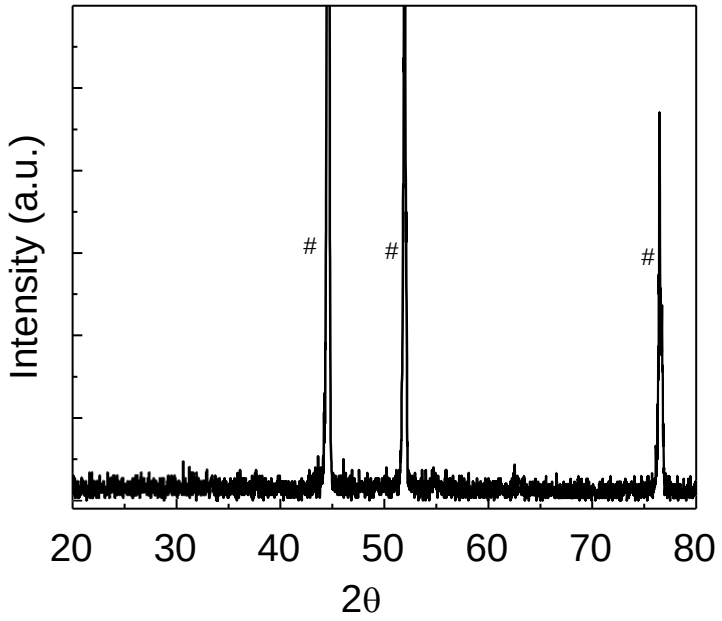

Fig.S1: X-ray diffraction pattern of as-deposited $CuCo(OH)_2$ nanosheet electrode

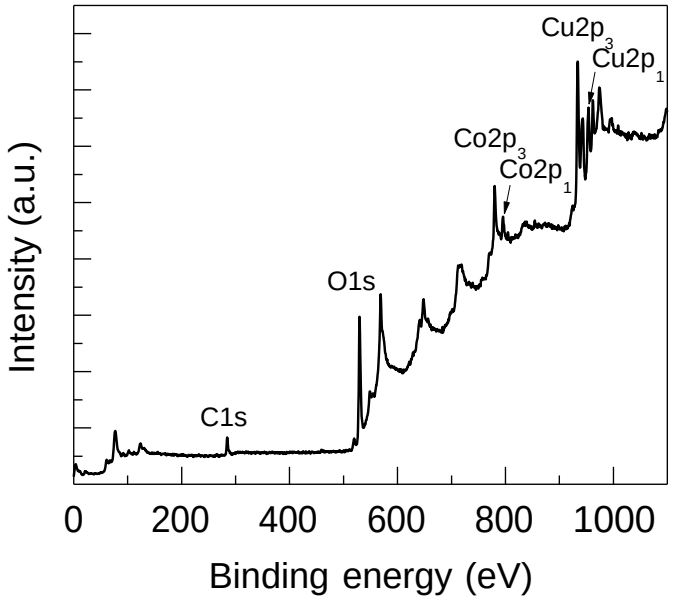

Fig. S2: XPS survey spectrum of $CuCo_2O_4$ nanosheet electrode.

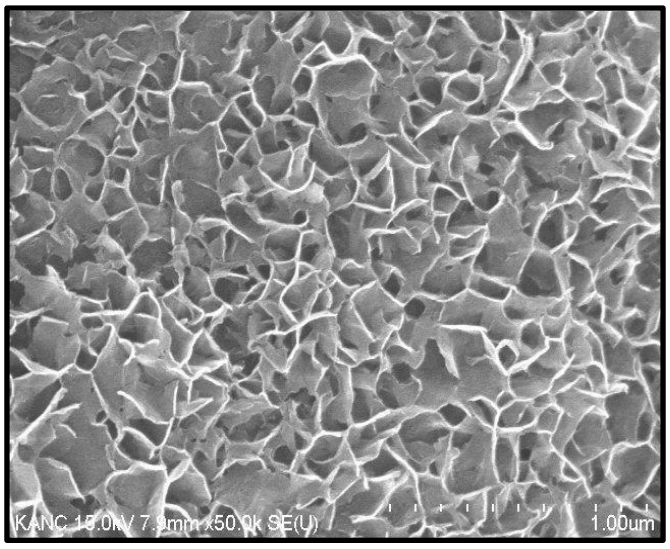

Fig. S3: As-deposited $CuCo(OH)_2$ nanosheet films

Table S1. Compositional analysis of the $CuCo_2O_4$ nanosheets.

Elements	**Cu**	**Co**	**O**
At %	12.68	27.0	60.32